Chemical Engineering Journal 280 (2015) 441–447

Contents lists available at ScienceDirect

Chemical Engineering Journal

journal homepage: www.elsevier.com/locate/cej

Two dimensional graphitic-phase C_3N_4 as multifunctional protecting layer for enhanced short-circuit photocurrent in ZnO based dye-sensitized solar cells

Dapeng Wu [a,b,*], Kun Cao [a], Fujuan Wang [a], Hongju Wang [a], Zhiyong Gao [a], Fang Xu [a], Yuming Guo [a,b], Kai Jiang [a,b,*]

[a] School of Chemistry and Chemical Engineering, Henan Normal University, Xinxiang, Henan 453007, PR China
[b] Collaborative Innovation Center of Henan Province for Green Motive Power and Key Materials, Henan Key Laboratory of Photovoltaic Materials, Henan Normal University, Xinxiang, Henan 453007, PR China

HIGHLIGHTS

- g-C_3N_4 was decorated on ZnO nanoparticles *via* an ultrasonic irradiation assisted monolayer dispersion.
- The g-C_3N_4 expands the absorption spectrum of ZnO photoanode to visible region.
- The stepwise energy gradient at the interface improves the injection efficiency.
- Large stride J_{sc} and *PCE* enhancements (~57% and ~20%) were demonstrated on Cell-ZnO–C_3N_4.

GRAPHICAL ABSTRACT

Two dimensional g-C_3N_4 was, for the first time, adopted in a solar energy conversion device and the DSSC with ZnO–C_3N_4 composite demonstrates a ~57% J_{sc} enhancement compared with that derives from pure ZnO.

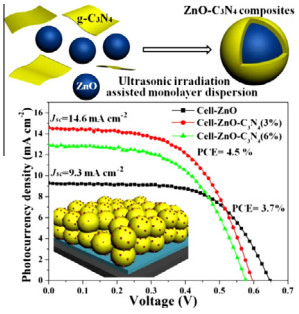

ARTICLE INFO

Article history:
Received 20 March 2015
Received in revised form 16 May 2015
Accepted 2 June 2015
Available online 10 June 2015

Keywords:
ZnO
g-C_3N_4
Ultrasonic irradiation
Monolayer dispersion
Dye-sensitized solar cells

ABSTRACT

Two dimensional graphitic-phase C_3N_4 (g-C_3N_4) was successfully coated as multifunctional protecting layer on ZnO nanoparticles *via* ultrasonic irradiation assisted monolayer dispersion. The as-prepared composites were applied as photoanode materials in dye-sensitized solar cells. Based on the optical and electrochemical measurements, the g-C_3N_4 stretches the absorption spectrum of the ZnO based photoanodes to visible region and enhances the harvesting of low energy photons. Moreover, the g-C_3N_4 with compatible band structure builds a stepwise energy gradient at the ZnO/C_3N_4/dye interface, which improves the injection efficiency of photo-generated electrons and leads to ~57% enhancement in the short-circuit photocurrent of Cell-ZnO–C_3N_4 (3%). Therefore, a high power conversion efficiency of 4.5% was demonstrated, indicating ~20% improvement compared with the pure ZnO based device (3.7%).

1. Introduction

Dye-sensitized solar cells (DSSCs) have been intensively studied for decades because of their low cost, high efficiency and facile preparation process [1–3]. Photoanode is one of the key

* Corresponding authors at: School of Chemistry and Chemical Engineering, Henan Normal University, Xinxiang, Henan 453007, PR China. Tel./fax: +86 37 3326209 (D. Wu and K. Jiang).
E-mail address: dpengwu@126.com (D. Wu).

http://dx.doi.org/10.1016/j.cej.2015.06.006
1385-8947/

components in the configuration and nano-sized TiO_2 is the most commonly used photoanode materials. Due to the similar electron band structure, excellent bulk electron mobility and the richest family of nanostructures, ZnO is also regarded as promising candidate for the photoanode in DSSC [4–6]. Although many researchers have been devoted to prepare various ZnO structures for DSSC application, the highest power conversion efficiency (*PCE*) of ZnO-based devices merely reaches to ~7.5%, which is far less than the TiO_2 based DSSCs with *PCE* of ~13% [7–10]. In addition, the ZnO nanoparticles are vulnerable in the ruthenium based dyes, because the acid function groups in the dye molecules can detach Zn^{2+} from the host lattice to form Zn^{2+}-dye agglomerations. The agglomerations on the ZnO surface not only result in low electron injection efficiency but also trigger massive charge recombination opportunities [11–13]. Therefore, surface modification with protecting layers such as SiO_2 Al_2O_3 or TiO_2 were widely adopted to enhance the stability of ZnO and suppress the charge recombination [14–17]. In these researches, the additional coating layers function as physical passivating layer to minimize the direct contact between ZnO and the dye molecules, which could significantly improve the fill factor (*FF*) and open circuit voltage (V_{oc}) of the devices. However, the introduced semiconducting or insulating layers could not directly improve the harvesting efficiency of the incident light and usually bring forth injection problem of the photo-generated electrons. Therefore, these strategies seldom increases the short circuit current (J_{sc}) of the devices.

Recently, two-dimensional crystals with thicknesses in atom scale attracted extensive attentions because of their excellent electronic, optical, and biocompatible properties [18–20]. Metal-free graphitic-phase C_3N_4 (g-C_3N_4) possesses graphite-like structure with layer distance of ~0.33 nm and band gap of ~2.69 eV [21]. Heretofore, g-C_3N_4 with different topological structures and g-C_3N_4 based heterogeneous materials have been applied in various fields [22]. The foremost research interests are focused on the photo-degradation for environmental remediation [23–31] and water splitting for H_2 fuel [32–34]. In addition, the potential application of g-C_3N_4 were also expanded to many territories such as adsorption [35], fuel cell [36], sensors [37], bio-imaging [38], and Li ion batteries [39]. However, so far as we know, g-C_3N_4 has been seldom studied to explore its potential application in solar energy conversion devices [40].

In this work, ZnO–C_3N_4 composites were prepared by an ultrasonic irradiation assisted monolayer dispersion and the effects of g-C_3N_4 coating layer on the performances of ZnO-based DSSCs were interpreted (Scheme 1). It was found that the g-C_3N_4 could expand the absorption spectra of ZnO based photoanodes to visible region and enhance the harvest of low energy photons. Moreover, the compatible band structure of g-C_3N_4 builds a stepwise energy gradient at the ZnO/C_3N_4/dye interface, which improves the injection efficiency of photo-generated electrons and finally leads to ~57% J_{sc} enhancement. Therefore, a higher *PCE* of 4.5% was demonstrated, indicating ~20% improvement compared with the pure ZnO based device.

2. Materials and methods

2.1. Materials preparation

2.1.1. Graphitic-phase C_3N_4

The g-C_3N_4 nano-sheet is prepared through an ultrasonic assisted liquid phase exfoliation. The bulk C_3N_4 was prepared by heating melamine at 550 °C for 2 h in N_2 atmosphere. 0.1 g of the yellowish product are grounded and ultrasonicated in 100 mL distilled water for 1 h and centrifuged for 15 min at 4000 rpm to remove the unexfoliated g-C_3N_4 and obtain the light yellow suspension for later use.

2.1.2. ZnO nanoparticles

The ZnO nanoparticles were prepared by decomposing $Zn(Ac)_2{\cdot}2H_2O$ in a solvothermal method. Briefly, 0.3 g $Zn(Ac)_2{\cdot}2H_2O$ was dispersed into 40 mL absolute ethanol. After stirring for 1 h, the suspension was transferred into 50 mL Teflon-lined autoclave and heated at 180 °C for 4 h. The white powder were rinsed with distilled water and absolute ethanol, and finally dried in vacuum for later use.

2.1.3. ZnO–C_3N_4 hybrid materials

The ZnO–C_3N_4 hybrid materials were prepared by monolayer dispersion method proposed by Zhu et al. and received a slight modification [41]. Typically, 0.2 g of ZnO nanoparticles were dispersed into appropriate volume of g-C_3N_4 suspension and the mixtures were placed in ultrasonic bath for 30 min and then stirred to volatilizate the water for about 2 days. The products were dried in vacuum for 3 h at 100 °C. The loading amount of the g-C_3N_4 was controlled be the volume of the g-C_3N_4 suspension. In addition, ZnO loaded with 3 wt.% and 6 wt.% g-C_3N_4 are named as ZnO–C_3N_4 (3%) and ZnO–C_3N_4 (6%).

2.2. Preparation of the photoanodes

Hydroxypropyl cellulose was added into diethylene glycol with a concentration of ~10 wt.% under magnetite stirring to yield

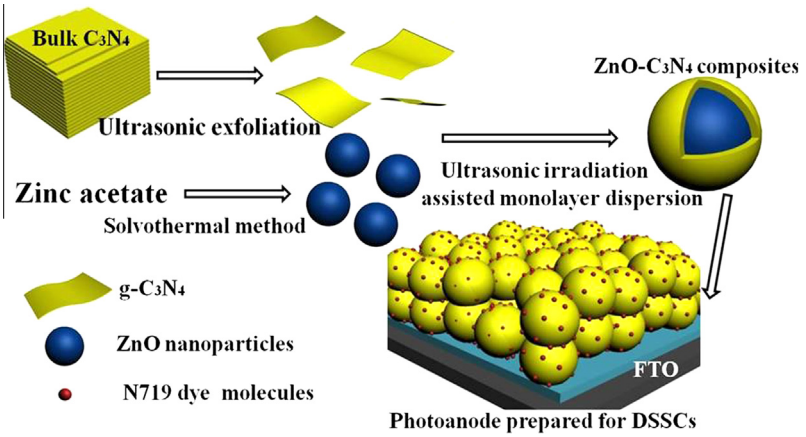

Scheme 1. Schematic illustration of the ultrasonic irradiation assisted monolayer dispersion to prepare the ZnO–C_3N_4 composites and their application as multifunctional protecting layer on the photoanode for DSSCs.

transparent paste for later use. The as-prepared paste was added into the ZnO–C_3N_4 (3%) and ZnO–C_3N_4 (6%) with appropriate ratio and stirred to obtain homogenous slurries. Doctor-blade method was adopted to deposit the slurries onto fluorine-doped tin oxide (FTO) glass substrate (TEC-8, LOF). After dried in air, the photoanodes were heated to 450 °C with a rate of 5 °C min^{-1} and maintained for 30 min. The film thicknesses were all controlled at ~12 μm. After cooled to 80 °C, the films were sensitized in a solution of cis-bis(isothiocyanato)bis(2,2′-bipyridy1-4,4′-dicarboxylate)ruthenium(II)bis-tetrabu-tylammoni-um (N719, Solaronix SA, Switzerland) in ethanol (3×10^{-4} M) for 1 h. The dyed films were then sandwiched together with platinized FTO counter electrodes and electrolyte was then injected into the cell from the edges by capillarity. The content of the electrolyte is 0.05 M LiI, 0.05 M I_2, 0.5 M 4-terbutylpyridine and 0.6 M 1-propyl-3-methylimidazolium iodiode (PMII) in 3-mathoxyproprionitrile.

2.3. Materials characterizations

The morphologies and structures of the products were characterized by field-emission scanning electron microscopy (FESEM, HITACHI, S4800), X-ray powder diffraction (XRD, Rigaku D/max-2500 diffractometer with Cu Kα radiation, $\lambda = 0.1542$ nm, 40 kV, 100 mA), transmission electron microscopy (TEM, FEI Tecnai F30), and Brunauer–Emmett–Teller (BET, Micrometrics ASAP 2010). The high-angle annular dark field scanning transmission electron microscopy (STEM-HAADF) was employed using the same TEM instrument, which is equipped with a scanning unit and a HAADF detector from Fischione (model 3000). Additionally, the compositional analysis of the microstructures was performed with the energy dispersive X-ray spectroscopy (EDS, EDAX Inc.) attachment on the Tecnai F30 during the TEM measurements.

2.4. Photovoltage measurements

Photocurrent–voltage (*I–V*) measurements were performed on a Keithley 4200 semiconductor characterization system using simulated AM 1.5 sunlight with an output power of 100 mW cm^{-2} produced by a solar simulator (Newport 69911). Incident monochromatic photo-to-electron conversion efficiency (IPCE) was recorded on a Keithley 2000 sourcemeter under the irradiation of a 150 W tungsten lamp with 1/4 m monochromator (Spectral Product DK240). The optical diffuse-reflection spectra were measured by spectrophotometer (HITACHI U-4100). Mott–Schottky spectra were obtained with Frequency Response Detector (FRD 100) and Potentiostat/Galvanostat Model 283 System (Princeton Applied Research). The potential was systematically varied between 1.00 and −1.00 V with the frequency of 1000 Hz by choosing Mott–Schottky technique template.

3. Results and discussion

The SEM image displayed in Fig. 1a shows the as-prepared ZnO nanoparticles have prism-like shapes and the particle size is about 20–50 nm. The TEM image in Fig. 1b shows well-defined lattice fringes and the interplanar spacing could be measured as ~0.26 nm, which corresponds to the (0001) plane. After coated with ~3% (wt) g-C_3N_4, many wrinkle-like patterns appear on each ZnO nanoparticle, which is obviously different from the clear surface condition of pure ZnO, indicating the homogenous coverage of g-C_3N_4 (Fig. 1c). As it is described in Zhu et al.'s pioneer work, the uniform coverage derives from monolayer dispersion of sheet-like g-C_3N_4 on the surface of ZnO nanoparticles and the driving force is the minimization of surface free energy [41]. As depicted in Fig. 1d, the HRTEM image taken from one of the nanoparticles clearly reveals the (0001) and $(01\bar{1}0)$ lattice planes of wurtzite structured ZnO with interplanar spacing of ~0.26 and ~0.28 nm, which could be further confirmed by the inset FFT dot patterns. In addition, very thin amorphous-like layer could be observed, which is distinctly different from the clear surface of pure ZnO, indicating g-C_3N_4 layer was coated on the ZnO surface. The thickness could be roughly measured as ~0.39 nm, suggesting the g-C_3N_4 layer was approximately coated with monolayer patterns. High-angle annular dark field scanning transmission electron microscopy (STEM-HAADF) was employed to compositionally analysis the composite (Fig. 1e). The energy dispersive X-ray spectrum shows the

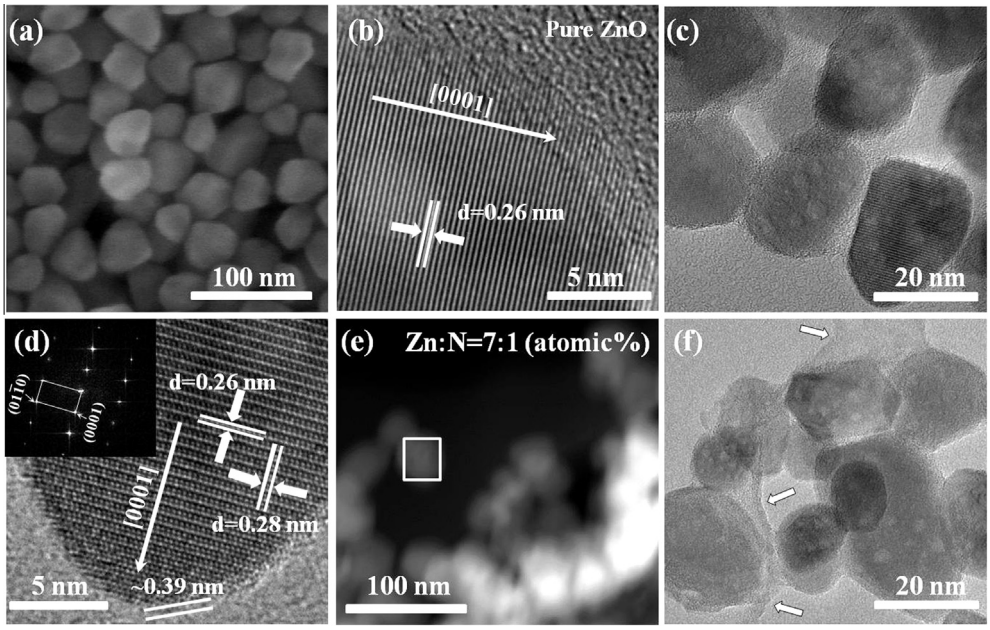

Fig. 1. (a) The SEM and (b) TEM images of as-prepared ZnO particles, (c and d) TEM images of the ZnO particles coated with 3% g-C_3N_4, the inset is Fast Fourier transform (FFT) patterns of the lattice fringes, (e) Zn/N atom ratio measured by energy dispersion analysis in the STEM-HAADF mode and (f) TEM image of the ZnO particles coated with 6% g-C_3N_4.

ratio between Zn and N in an individual particle (marked in white square) is 7/1, indicating the dosage of g-C_3N_4 in ZnO is ~3.88% (wt) which is in accord with our experimental dosage. Fig. 1f shows the TEM image of ZnO–C_3N_4 (6%). In addition to the g-C_3N_4 coated on ZnO nanoparticles, individual sheet-like patterns could be also observed (denoted by the arrows), implying excessive g-C_3N_4 was added for the surface modification.

The crystallographic structures of the samples are confirmed by the X-ray diffraction (XRD) and displayed in Fig. 2. The ZnO nanoparticle is highly crystallized and of pure wurtzite phase. In addition, no obvious characteristic diffractions peaks belonging to g-C_3N_4 is detected in the ZnO–C_3N_4 composites (3% and 6%), indicating the g-C_3N_4 is uniformly coated on the ZnO nanoparticles. As described in previous work, the composite with 6% g-C_3N_4 dosage usually exhibits a weak g-C_3N_4 peak. In our case, the ultrasonic irradiation could better disperse the g-C_3N_4 monolayer on ZnO nanoparticles, which diminishes the characteristic diffraction peak of g-C_3N_4. The samples are further investigated by Fourier Transform Infrared (FT-IR) spectra (Fig. 3). For g-C_3N_4, the peaks centered at 1243, 1324, 1415, 1421, 1564, and 1645 cm^{-1} dominate the spectrum, corresponding to the typical stretching mode of CN heterocycles. Additionally, the characteristic breathing mode of s-triazine ring is observed at 807 cm^{-1}.[41,42] As for ZnO–C_3N_4 composites, the main characteristic peaks belonging to g-C_3N_4 are suppressed, indicating the bond strengths of intrinsic C–N bonds are weakened. Moreover, new prominent signals at 1156 cm^{-1} corresponding to the C–O bonding are observed, which indicates that new bonding models are formed between the C and O atoms respectively from g-C_3N_4 and ZnO. The FT-IR analysis demonstrates that a conjugated system was built between g-C_3N_4 and ZnO, which may be of great significance for the charge migration in the hybrid material.

Pure ZnO and ZnO with different g-C_3N_4 dosages (3% and 6%) were respectively deposited on FTO substrate as photoanodes for DSSC application. The photovoltaic performances of the as-prepared DSSCs were tested under one sun illumination with a power density of 100 mW cm^{-2}. Fig. 4 shows the typical *I–V* curves of the DSSCs and the detailed photovoltage characteristics are listed in Table 1. Cell-ZnO shows J_{sc} of 9.3 mA cm^{-2}, V_{oc} of 646 mV and *FF* of 61.6%, which gives a *PCE* of 3.7%. Although the *FF* and V_{oc} of Cell-ZnO–C_3N_4 (3%) are decreased, it demonstrates a much higher J_{sc} of 14.6 mA cm^{-2}, indicating ~57% enhancement compared with Cell-ZnO, which leads to a higher *PCE* of 4.5%.

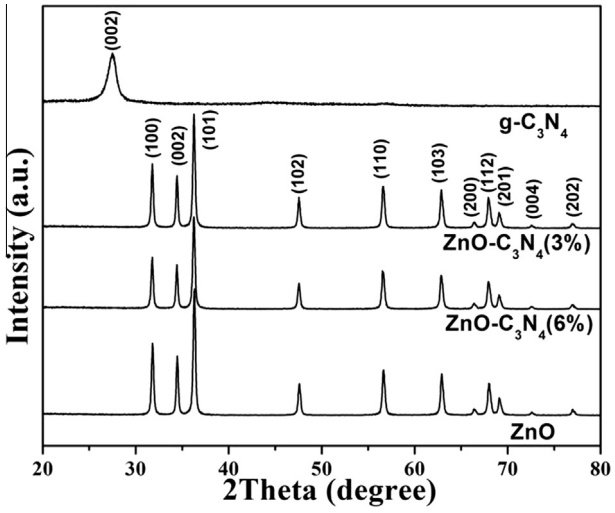

Fig. 2. The XRD patterns of the as-prepared g-C_3N_4, ZnO–C_3N_4 (3%), ZnO–C_3N_4 (6%) and ZnO nanoparticle.

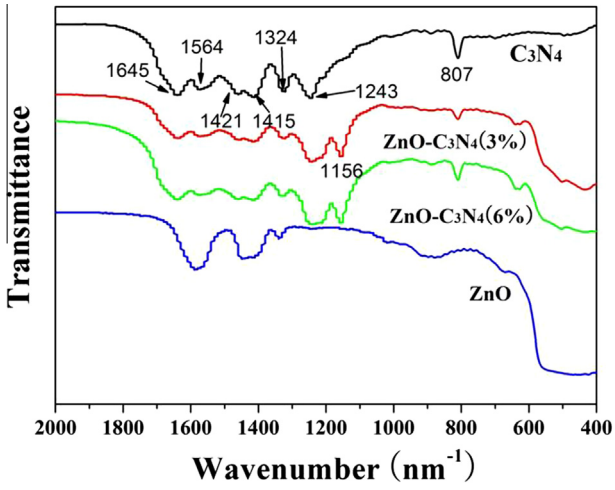

Fig. 3. FT-IR spectra of the as-prepared g-C_3N_4, ZnO–C_3N_4 (3%), ZnO–C_3N_4 (6%) and ZnO nanoparticle.

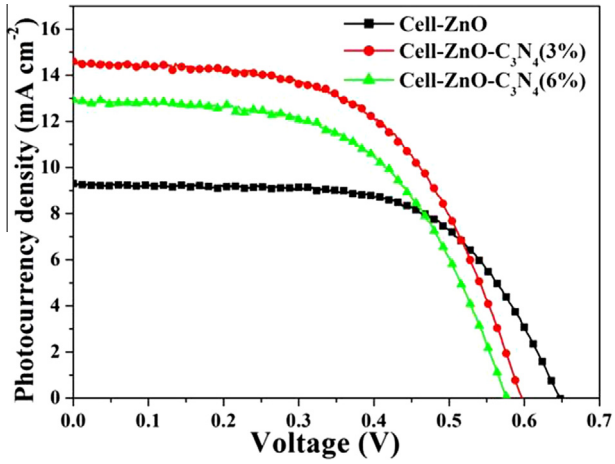

Fig. 4. The current–voltage characteristics measured under one sun (100 mW cm^{-2}) of the as-prepared DSSCs.

Table 1
The photovoltage characteristics for DSSCs based on the pure ZnO, ZnO–C_3N_4 (3%) and ZnO–C_3N_4(6%).

Cells	J_{sc} (mA cm^{-2})	V_{oc} (mV)	*FF* (%)	*PCE* (%)	Dye absorb. (mol cm^{-2})
ZnO	9.3	646	61.6	3.7	2.5×10^{-7}
ZnO–C_3N_4 (3%)	14.6	596	51.7	4.5	2.4×10^{-7}
ZnO–C_3N_4 (6%)	12.9	576	48.4	3.6	2.2×10^{-7}

Thanks to the g-C_3N_4 coating layer, the J_{sc} of Cell-ZnO–C_3N_4 (6%) is also improved. Nevertheless, the greatly reduced *FF* and V_{oc} result in a lower *PCE* of 3.6%. It is obvious that the higher *PCE* of Cell-ZnO–C_3N_4 (3%) derives from the substantially improved J_{sc}.

The J_{sc} variation is complicated and the affecting factors are rather multiple-folded. Generally, the J_{sc} is determined by the light harvesting efficiency of the photoanode, the injection and collection efficiencies of the photoelectrons [43,44]. UV–vis absorption spectra of the photoanodes before and after dye loading are presented in Fig. 5a and b. Without dye loading, the ZnO film shows clear absorption onset at ~380 nm which corresponds to the intrinsic band edge absorption of ZnO. Due to the incorporation

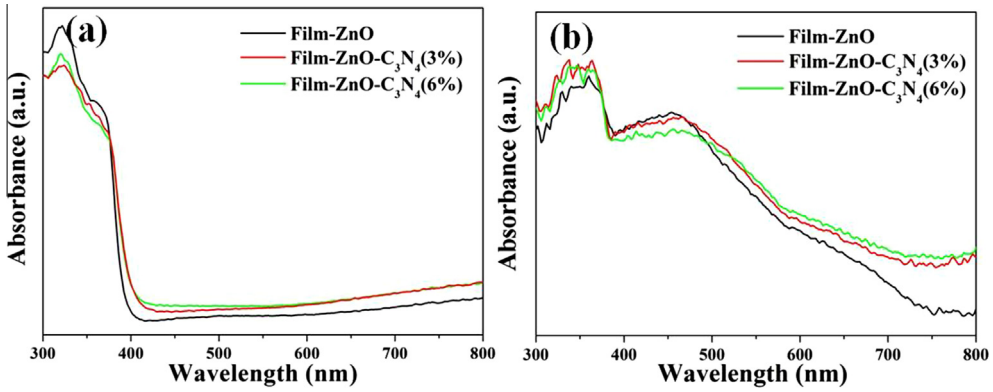

Fig. 5. The UV–vis absorption spectra of the photoanode films (a) before and (b) after dye loading.

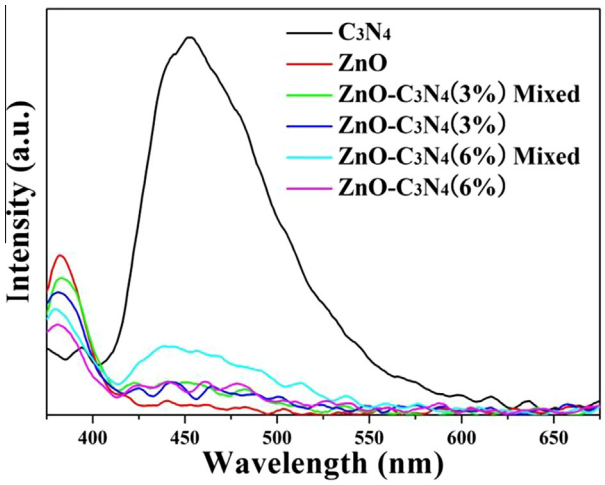

Fig. 6. Photoluminescence spectra of the g-C_3N_4, ZnO and the composites prepared through monolayer dispersion and directly mixed ZnO and g-C_3N_4.

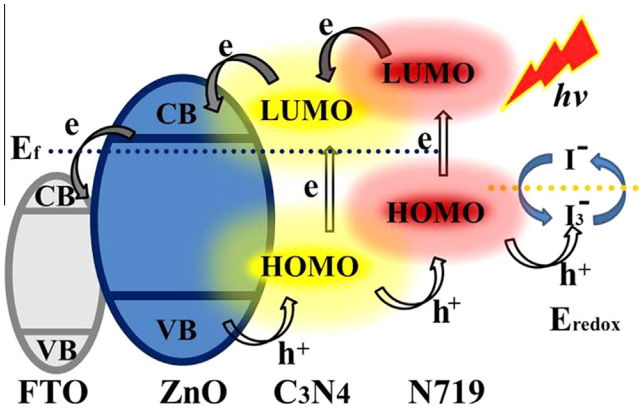

Scheme 2. Illustration of the stepwise energy levels built at the ZnO/C_3N_4/dye interface.

of g-C_3N_4, Film-ZnO–C_3N_4 (3%) shows evident red shift and the absorbance was also enhanced in the range of 400–800 nm, which suggests that the band gaps of these composites are reduced [45]. Compared with Film-ZnO–C_3N_4 (3%), no obvious band shift is detected in Film-ZnO–C_3N_4 (6%). Moreover, the absorbance in the region of 400–600 nm is slightly enhanced as increasing the g-C_3N_4 dosage. After loaded with N719 dyes, Film-ZnO–C_3N_4 (3%) shows similar absorbance in the range of 400–600 nm corresponding to the intrinsic absorption of N719, which indicates the low g-C_3N_4 dosage won't affect the dye loading amount (Table 1). Moreover, the Film-ZnO–C_3N_4 (3%) shows higher absorbance in the range from 500 to 00 nm, implying more visible light could be trapped in the photoanode as g-C_3N_4 was introduced. However, as increasing the g-C_3N_4 dosage, the absorbance in the range of 550–800 nm is further promoted for Film-ZnO–C_3N_4 (6%). However, the absorbance in the range of 400–550 nm is greatly reduced, which proves the dye loading amount is reduced (Table 1). In order to interpret the differences in the dye loading amount of the photoanodes, the surface area of the composites were measured as 39.1 and 40.3 $m^2\ g^{-1}$ for ZnO–C_3N_4 (3%) and ZnO–C_3N_4 (6%) respectively, which are marginally increased from that of pure ZnO (38.6 $m^2\ g^{-1}$). However, the dye loading amount of the photoanodes are slightly reduced as increasing the dosage of g-C_3N_4 (Table 1). Therefore, it could be concluded that the introduced g-C_3N_4 didn't help to increase the dye loading amount of the photoanodes but increase the light harvesting at the longer wavelength range (500–800 nm), which finally leads to the J_{sc} enhancement.

In addition, the band gap of g-C_3N_4 is 2.69 eV, and the highest occupied molecular orbital (HOMO) and lowest unoccupied molecular orbital (LUMO) potentials of g-C_3N_4 are −1.12 and 1.57 eV, respectively [21]. Therefore, when coated on the ZnO surface, a stepwise band alignment could be built, which facilitates the photoelectron injection and the hole scavenge of the redox couples. The band alignment between ZnO and g-C_3N_4 could be verified by the photoluminescence (PL) spectra [25,27,31]. The PL curves of pristine g-C_3N_4, ZnO, and composites including ZnO–C_3N_4 (3%), ZnO–C_3N_4 (6%), ZnO–C_3N_4 (3%, mixed) and ZnO–C_3N_4 (6%, mixed) are shown in Fig. 6. The emission peak of pristine g-C_3N_4 appears at ~450 nm (denoted as Vis-peaks), which is attributed to the band edge emission of g-C_3N_4. While, the peaks centered at ~380 nm (denoted as UV-peaks) represent the near-band-edge recombination of ZnO. Compared with the sample directly mixed with 3% g-C_3N_4, the UV-peak intensity of ZnO–C_3N_4 (3%) is further suppressed, indicating the charge transfer between ZnO and g-C_3N_4 is promoted. Similarly, with same g-C_3N_4 dosage level, ZnO–C_3N_4 (6%) shows much lower Vis-peak than ZnO–C_3N_4 (6%, mixed). The quenching of both the UV- and visible-emissions demonstrate the effective separation of photogenerated electrons and holes at the ZnO/C_3N_4 interface [46]. As displayed in Scheme 2, an energy gradient could be built at the ZnO/C_3N_4/dye interface due to the band alignment, which enhances migration of the charge carriers and the injection efficiency of photogenerated electrons.

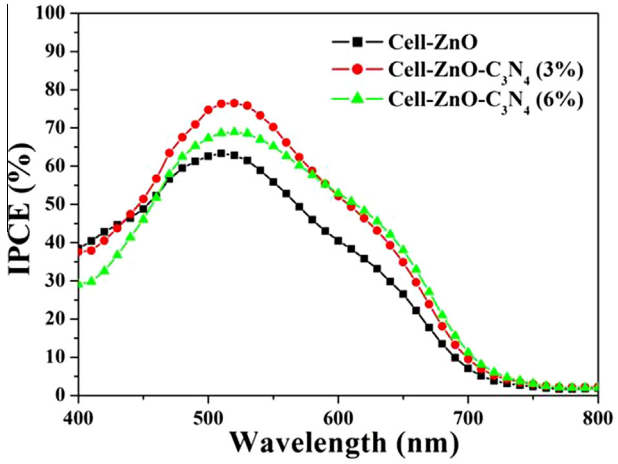

Fig. 7. Incident photon to current efficiency (IPCE) spectra of the as-prepared DSSCs.

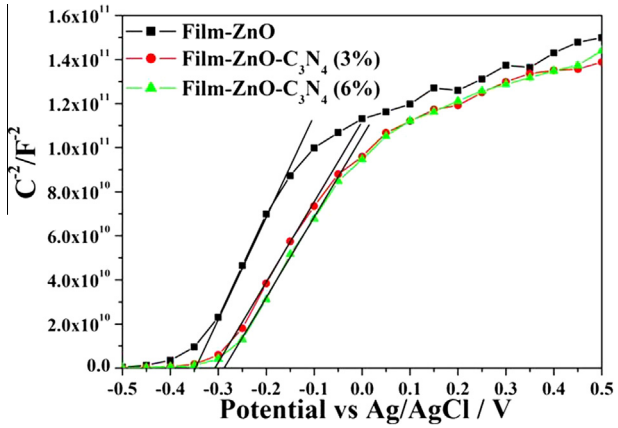

Fig. 8. Mott–Schottky spectra of the photoanode films without N719 sensitization.

Fig. 7 shows the incident photon to current efficiency (*IPCE*) spectra in function of wavelength, which directly reflects the J_{sc} variation. Cell-ZnO–C_3N_4 (3%) shows much higher *IPCE* value than Cell-ZnO, especially in the range of 550–800 nm. In addition, the *IPCE* in the range of 600–700 nm is enhanced for Cell-ZnO–C_3N_4 (6%) because more g-C_3N_4 is decorated on the photoanode. However, the *IPCE* in the range of 400–500 nm is decreased, which matches well with the optical and dye uptake measurements.

It should be noticed that, for Cell-ZnO–C_3N_4 (3%), the ~57% J_{sc} augment only leads to ~20% enhancement in *PCE*, which obviously derives from the reduced *FF* and V_{oc} compared with Cell-ZnO. As indicated in previous literature, the low *FF* mainly results from the increased series resistance of the cell [15]. Considering the g-C_3N_4 was wrapped on each ZnO nanoparticle, the additional coating layer inevitably increases the series resistance of photoanode. Moreover, the V_{oc} of the devices could be expressed according to Eq. (1), [47]

$$V_{OC} = \frac{E_{cb}}{q} + \frac{kT}{q}\ln\left(\frac{n}{N_{cb}}\right) - \frac{E_{redox}}{q} \quad (1)$$

where E_{cb} is the conduction band edge, E_{redox} is the energy level of redox couples in the electrolyte, k_bT is the thermal energy, n_c is the free electrons density in the conduction band and N_c is the effective density of conduction band states. The sum of first two items in Eq. (1) is the quasi Fermi energy level (E_f) of the photoanode. Therefore, the V_{oc} is determined by the voltage gradient between the E_f and the E_{redox} [48]. Moreover, E_f is greatly affected by the variation of E_{cb}. As shown in Fig. 5a, the red shift of absorption curve indicates the band gap of the ZnO–C_3N_4 composites are reduced, which is usually associated with the downward shift of E_{cb}. Thermodynamically, the lower E_{cb} will lead to a lower E_f position and reduce the V_{oc} of DSSC. In addition, the Mott–Schottky analysis on the flat potential is a powerful method to directly indicate the E_f shift [49,50]. As shown in Fig. 8, the ZnO–C_3N_4 curves are shifted to positive potential range compared with that of pure ZnO, suggesting the g-C_3N_4 decoration leads to a downward E_f shift of the photoanode. Considering the E_{redox} usually remains unchanged, the V_{oc} of corresponding ZnO–C_3N_4 based DSSCs are decreased accordingly.

4. Conclusions

Two dimensional g-C_3N_4 was incorporated as multifunctional protecting layer on ZnO nanoparticles *via* a monolayer dispersion method. The as-prepared ZnO–C_3N_4 (3%) composite shows enhanced photovoltaic performances than pure ZnO when used in DSSCs. Based on the optical and electrochemical investigations, the enhancement could be ascribed to the following reasons: (1) the g-C_3N_4 reduces the band gap of the composite, which expands the absorption spectrum and enhances the light harvesting of the photoanode, (2) the compatible band structure of g-C_3N_4 builds stepwise energy gradient at ZnO/C_3N_4/dye interface, which improves the injection efficiency of photo-generated electrons, (3) the g-C_3N_4 may also function as a physical barrier layer to avoid the direct contact between the ZnO and the acid dye molecules to alleviate the corrosion of ZnO surface. In addition, the Achilles' Heel is that the g-C_3N_4 layer increases the series resistance and decreases the E_f of the photoanode, which results in lower *FF* and V_{oc}. Nevertheless, due to great J_{sc} enhancement (~57%), Cell-ZnO–C_3N_4 (3%) demonstrates higher *PCE* of 4.5%, indicating ~20% improvement compared with Cell-ZnO. Based on the intrinsic qualities such as suitable band structure, ultrathin thickness, chemical and photo-stability, environmental benign and low cost, g-C_3N_4 may be further applied as sensitizers, conducting materials or interfacing layers in other solar energy conversion devices.

Acknowledgments

This work is supported by National Natural Science Foundation of China (61204078, 61176004 and U1304505), Program for Changjiang Scholars and Innovative Research Team in University (PCSIRT) (Department of education, P.R. China), Program for Innovative Research Team (in Science and Technology) in University of Henan Province (No. 13IRTSTHN026), Basic and Frontier Research Programs of Henan Province (No. 142300410420) and Key Project of Science and Technology of Henan Province (Nos. 13A150517 and 14A150002).

References

[1] B. O'Regan, M. Gratzel, A low-cost, high-efficiency solar cell based on dye-sensitized colloidal TiO_2 films, Nature 353 (1991) 737–740.
[2] A. Yella, H.W. Lee, H.N. Tsao, Porphyrin-sensitized solar cells with cobalt(II/III)-based redox electrolyte exceed 12 percent efficiency, Science 334 (2011) 629–634.
[3] J. Du, J. Qi, D. Wang, Z. Tang, Facile synthesis of Au@TiO_2 core–shell hollow spheres for dye-sensitized solar cells with remarkably improved efficiency, Energy Environ. Sci. 5 (2012) 6914–6918.
[4] P. Tiwana, P. Docampo, M.B. Johnston, H.J. Snaith, L.M. Herz, Electron mobility and injection dynamics in mesoporous ZnO, SnO_2, and TiO_2 films used in dye-sensitized solar cells, ACS Nano 5 (2011) 5158–5166.
[5] Q.F. Zhang, C.S. Dandeneau, X.Y. Zhou, G.Z. Cao, ZnO nanostructures for dye-sensitized solar cells, Adv. Mater. 21 (2009) 4087–4108.
[6] L. Liu, L. Fu, Y. Liu, Y. Liu, P. Jiang, S. Liu, M. Gao, Z. Tang, Bioinspired synthesis of vertically aligned ZnO nanorod arrays: toward greener chemistry, Cryst. Growth Des. 9 (2009) 4793–4796.

[7] N. Memarian, I. Concina, A. Braga, S.M. Rozati, A. Vomiero, G. Sberveglieri, Hierarchically assembled ZnO nanocrystallites for high-efficiency dye-sensitized solar cells, Angew. Chem. Int. Ed. 50 (2011) 12321–12325.

[8] Z.H. Dong, X.Y. Lai, J.E. Halpert, N.L. Yang, L.X. Yi, J. Zhai, D. Wang, Z.Y. Tang, L. Jiang, Accurate control of multishelled ZnO hollow microspheres for dye-sensitized solar cells with high efficiency, Adv. Mater. 24 (2012) 1046–1049.

[9] X.H. Lu, Y.Z. Zheng, S.Q. Bi, Y. Wang, X. Tao, L.M. Dai, J.F. Chen, Multidimensional ZnO architecture for dye-sensitized solar cells with high-efficiency up to 7.35%, Adv. Energy Mater. 0 (2014) 1301802.

[10] D.P. Wu, Z.Y. Gao, F. Xu, J.L. Chang, W.G. Tao, J.J. He, S.Y. Gao, K. Jiang, Hierarchical ZnO aggregates assembled by orderly aligned nanorods for dye-sensitized solar cells, CrystEngComm 15 (2013) 1210–1217.

[11] J.A. Anta, E. Guillén, R. Tena-Zaera, ZnO-based dye-sensitized solar cells, J. Phys. Chem. C 116 (2012) 11413–11425.

[12] R. Gao, Y.X. Cui, X.J. Liu, L.D. Wang, G.Z. Cao, A ZnO nanorod/nanoparticle hierarchical structure synthesized through a facile in situ method for dyesensitized solar cells, J. Mater. Chem. A 2 (2014) 4765–4770.

[13] Q.F. Zhang, T.P. Chou, B. Russo, S.A. Jenekhe, G.Z. Cao, Aggregation of ZnO nanocrystallites for high conversion efficiency in dye-sensitized solar cells, Angew. Chem. Int. Ed. 47 (2008) 2402–2406.

[14] K. Park, Q.F. Zhang, B.B. Garcia, X.Y. Zhou, Y. Jeong, G.Z. Cao, Effect of an ultrathin TiO_2 layer coated on submicrometer-sized ZnO nanocrystallite aggregates by atomic layer deposition on the performance of dye-sensitized solar cells, Adv. Mater. 22 (2010) 2329–2332.

[15] D.P. Wu, Z.Y. Gao, F. Xu, Z.P. Shi, W.G. Tao, K. Jiang, Nanosheet-based hierarchical ZnO structure decorated with TiO_2 particles for enhanced performance in dye-sensitized solar cell, CrystEngComm 14 (2012) 7934–7941.

[16] Y. Lou, S. Yuan, Y. Zhao, P. Hu, Z. Wang, M. Zhang, L. Shi, D. Li, A simple route for decorating TiO_2 nanoparticle over ZnO aggregates dye-sensitized solar cell, Chem. Eng. J. 229 (2013) 190–196.

[17] L.E. Greene, M. Law, B.D. Yuhas, P.D. Yang, ZnO–TiO_2 core–shell nanorod/P3HT solar cells, J. Phys. Chem. C 111 (2007) 18451–18456.

[18] K.S. Novoselov, D. Jiang, F. Schedin, T.J. Booth, V.V. Khotkevich, S.V. Morozov, A.K. Geim, Two-dimensional atomic crystals, Proc. Natl. Acad. Sci. USA 102 (2005) 10451–10453.

[19] A.K. Geim, K.S. Novoselov, The rise of graphene, Nat. Mater. 6 (2007) 183–191.

[20] K.P. Loh, Q. Bao, G. Eda, M. Chhowalla, Graphene oxide as a chemically tunable platform for optical applications, Nat. Chem. 2 (2010) 1015–1024.

[21] X.C. Wang, K. Maeda, A. Thomas, K. Takanabe, G. Xin, J.M. Carlsson, K. Domen, M. Antonietti, A metal-free polymeric photocatalyst for hydrogen production from water under visible light, Nat. Mater. 8 (2009) 76–80.

[22] G.G. Zhang, M.W. Zhang, X.X. Ye, X.Q. Qiu, S. Lin, X.C. Wang, Iodine modified carbon nitride semiconductors as visible light photocatalysts for hydrogen evolution, Adv. Mater. 26 (2014) 805–809.

[23] S.P. Wang, C.J. Li, T. Wang, P. Zhang, A. Li, J.L. Gong, Controllable synthesis of nanotube-type graphitic C_3N_4 and their visible-light photocatalytic and fluorescent properties, J. Mater. Chem. A 2 (2014) 2885–2890.

[24] H. Wang, X. Zhang, J. Xie, J. Zhang, P. Ma, B.C. Pan, Y. Xie, Structural distortion in graphitic-C 3 N 4 realizing an efficient photoreactivity, Nanoscale 7 (2015) 5152–5156.

[25] Z. Tong, D. Yang, T. Xiao, Y. Tian, Z. Jiang, Biomimetic fabrication of g-C_3N_4/TiO_2 nanosheets with enhanced photocatalytic activity toward organic pollutant degradation, Chem. Eng. J. 260 (2015) 117–125.

[26] L.F. Ming, H. Yue, L.M. Xu, F. Chen, Hydrothermal synthesis of oxidized g-C_3N_4 and its regulation of photocatalytic activity, J. Mater. Chem. A 2 (2014) 19145–19149.

[27] Y. Zang, L. Li, X. Li, R. Lin, G. Li, Synergistic collaboration of g-C_3N_4/SnO_2 composites for enhanced visible-light photocatalytic activity, Chem. Eng. J. 246 (2014) 277–286.

[28] X. Zhang, J. Hu, H. Jiang, Facile modification of a graphitic carbon nitride catalyst to improve its photoreactivity under visible light irradiation, Chem. Eng. J. 256 (2014) 230–237.

[29] X. Wang, L. Wang, F. Zhao, C. Hu, Y. Zhao, Z. Zhang, S. Chen, G. Shi, L. Qu, Monoatomic-thick graphitic carbon nitride dots on graphene sheets as an efficient catalyst in the oxygen reduction reaction, Nanoscale 7 (2015) 3035–3042.

[30] D. Chen, K. Wang, T. Ren, H. Ding, Y.F. Zhu, Synthesis and characterization of the ZnO/mpg-C_3N_4 heterojunction photocatalyst with enhanced visible light photoactivity, Dalton Trans. 43 (2014) 13105–13114.

[31] J. Zhou, M. Zhang, Y.F. Zhu, Preparation of visible light-driven g-C_3N_4@ZnO hybrid photocatalyst via mechanochemistry, Phys. Chem. Chem. Phys. 16 (2014) 17627–17633.

[32] Y.J. Zhou, L.X. Zhang, J.J. Liu, X.Q. Fan, B.Z. Wang, M. Wang, W.C. Ren, J. Wang, M.L. Li, J.L. Shi, Brand new P-doped g-C3N4: enhanced photocatalytic activity for H2 evolution and rhodamine B degradation under visible light, J. Mater. Chem. A 3 (2015) 3862–3867.

[33] D.D. Zheng, C. Huang, X. Wang, Post-annealing reinforced hollow carbon nitride nanospheres for hydrogen photosynthesis, Nanoscale 7 (2015) 465–470.

[34] S.W. Cao, J.G. Yu, g-C_3N_4-based photocatalysts for hydrogen generation, J. Phys. Chem. Lett. 5 (2014) 2101–2107.

[35] R. Hu, X. Wang, S. Dai, D. Shao, T. Hayat, A. Alsaedi, Application of graphitic carbon nitride for the removal of Pb(II) and aniline from aqueous solutions, Chem. Eng. J. 260 (2015) 469–477.

[36] Y. Zheng, Y. Jiao, J. Chen, J. Liu, J. Liang, A.J. Du, W.M. Zhang, Z.H. Zhu, S.C. Smith, M. Jaroniec, G.Q. Lu, S.Z. Qiao, Nanoporous graphitic-C_3N_4@carbon metal-free electrocatalysts for highly efficient oxygen reduction, J. Am. Chem. Soc. 133 (2011) 20116–20119.

[37] X.J. She, H. Xu, Y.G. Xu, J. Yan, J.X. Xia, L. Xu, Y.H. Song, Y. Jiang, Q. Zhang, H.M. Li, Exfoliated graphene-like carbon nitride in organic solvents: enhanced photocatalytic activity and highly selective and sensitive sensor for the detection of trace amounts of Cu^{2+}, J. Mater. Chem. A 2 (2014) 2563–2570.

[38] X.D. Zhang, X. Xie, H. Wang, J.J. Zhang, B.C. Pan, Y. Xie, Enhanced photoresponsive ultrathin graphitic-phase C_3N_4 nanosheets for bioimaging, J. Am. Chem. Soc. 135 (2013) 18–21.

[39] L.L. Tian, X.Y. Wei, Q.C. Zhuang, C.H. Jiang, C. Wu, G.Y. Ma, X. Zhao, Z.M. Zong, S.G. Sun, Bottom-up synthesis of nitrogen-doped graphene sheets for ultrafast lithium storage, Nanoscale 6 (2014) 6075–6083.

[40] P. Wu, J. Wang, J. Zhao, L.J. Guo, F.E. Osterloh, Structure defects in g-C_3N_4 limit visible light driven hydrogen evolution and photovoltage, J. Mater. Chem. A 2 (2014) 20338–20344.

[41] Y.J. Wang, R. Shi, J. Lin, Y.F. Zhu, Enhancement of photocurrent and photocatalytic activity of ZnO hybridized with graphite-like C_3N_4, Energy Environ. Sci. 4 (2011) 2922–2929.

[42] S. Kumar, A. Baruah, S. Tonda, B. Kumar, V. Shanker, B. Sreedhar, Cost-effective and eco-friendly synthesis of novel and stable N-doped ZnO/g-C_3N_4 core–shell nanoplates with excellent visible-light responsive photocatalysis, Nanoscale 6 (2014) 4830–4842.

[43] D.P. Wu, Y. Wang, H. Dong, F. Zhu, S.Y. Gao, K. Jiang, L.M. Fu, J.P. Zhang, D.S. Xu, Hierarchical TiO_2 microspheres comprised of anatase nanospindles for improved electron transport in dyesensitized solar cells, Nanoscale 5 (2013) 324–330.

[44] D.P. Wu, F. Zhu, J.M. Li, H. Dong, Q. Li, K. Jiang, D.S. Xu, Monodisperse TiO_2 hierarchical hollow spheres assembled by nanospindles for dye-sensitized solar cells, J. Mater. Chem. 22 (2012) 11665–11671.

[45] J. Wang, W.D. Zhang, Modification of TiO_2 nanorod arrays by graphite-like C_3N_4 with high visible light photoelectrochemical activity, Electrochim. Acta 71 (2012) 10–16.

[46] W. Liu, M. Wang, C. Xu, S. Chen, Facile synthesis of g-C_3N_4/ZnO composite with enhanced visible light photooxidation and photoreduction properties, Chem. Eng. J. 209 (2012) 386–393.

[47] T. Marinado, K. Nonomura, J. Nissfolk, M.K. Karlsson, D.P. Hagberg, L. Sun, S. Mori, A. Hagfeldt, How the nature of triphenylamine-polyene dyes in dye-sensitized solar cells affects the open-circuit voltage and electron lifetimes, Langmuir 26 (2009) 2592–2598.

[48] Z. Ning, Y. Fu, H. Tian, Improvement of dye-sensitized solar cells: what we know and what we need to know, Energy Environ. Sci. 3 (2010) 1170–1181.

[49] J.J. He, D.P. Wu, Z.Y. Gao, F. Xu, S.W. Jiang, S. Zhang, K. Cao, Y.M. Guo, K. Jiang, Graphene sheets anchored with high density TiO_2 nanocrystals and their application in quantum dot-sensitized solar cells, RSC Adv. 4 (2014) 2068–2072.

[50] F. Zhu, P.P. Zhang, X.J. Wu, L.M. Fu, J.P. Zhang, D.S. Xu, The origin of higher open-circuit voltage in Zn-doped TiO_2 nanoparticle-based dye-sensitized solar cells, ChemPhysChem 13 (2012) 3731–3737.